IEEE Access
Multidisciplinary ⋮ Rapid Review ⋮ Open Access Journal

Received 15 March 2024, accepted 27 March 2024, date of publication 1 April 2024, date of current version 15 April 2024.

Digital Object Identifier 10.1109/ACCESS.2024.3383836

RESEARCH ARTICLE

Illumination Induced Negative Differential Resistance in InGaAs Avalanche Photodiode

AFSHAN KHALIQ[1,2], XINYI ZHOU[1], HONG-YU CHAI[3], MUNIR ALI[1,4], HAO WU[1,5], OUSSAMA GASSAB[1,6], (Member, IEEE), HONG LIU[1], DUO XIAO[1], XIAO-GUANG YANG[3], AND SICHAO DU[1,6]

[1]Laboratory of Single-Photon Detection and Imaging Techniques, Zhejiang Engineering Research Center for Edge Intelligence Technology and Equipment, School of Information and Electrical Engineering, Hangzhou City University, Hangzhou, Zhejiang 310015, China
[2]Department of Physics, Zhejiang Normal University, Jinhua 321004, China
[3]Institute of Semiconductors, Chinese Academy of Sciences, Beijing 100083, China
[4]School of Micro-Nano Electronics, ZJU-Hangzhou Global Scientific and Technological Innovation Center, ZJU-UIUC Joint Institute, Zhejiang University, Hangzhou 310027, China
[5]College of Optical Science and Engineering, Zhejiang University, Hangzhou, Zhejiang 310027, China
[6]College of Information Science and Electronic Engineering, Zhejiang University, Hangzhou, Zhejiang 310027, China

Corresponding authors: Sichao Du (sichaodu@zju.edu.cn), Xiao-Guang Yang (xgyang@semi.ac.cn), and Duo Xiao (xiaod@hzcu.edu.cn)

This work was supported in part by the Young Talents Plan of Zhejiang University City College under Grant 202000-581832, in part by the Special Project for Improving Level of Local Universities in Zhejiang Province under Grant 202000-584102, in part by the Scientific Research Fund for Fostering Young Teachers under Grant 202000-581509-015, and in part by the Innovation Fund for High-Level Returned Overseas Scholars in Hangzhou under Grant 202000-591807.

ABSTRACT This work presents a novel InGaAs/InP avalanche photodiode, fabricated in the separate absorption, grading, charge, and multiplication configuration operated at non-cryogenic conditions under low-frequency ramp gating. An optimized three stage InP multiplication layer of $1\mu m$ thickness offers an extended linear mode operation by reducing the punch-through voltage, and indefinitely increasing the avalanche threshold voltage. A large background dark current is observed following steady, and linear multiplication in approximately direct relationship with the ramp gating. For 1310 nm short-wave infrared, normal incidence pulsed illumination at instant-to-peak voltage ratios of (0.11, 0.2, 0.6, 0.89, 0.98, 0.9), a sort of negative differential resistance is incorporated into the device in a qualitative sense, owing to the illumination induced switching/variations in the intrinsic values of electron, and hole avalanche coefficients in the multiplication region. Under fixed illumination, an interesting deduction from the transient photo response is the slow quenching phenomenon prolonging $\sim 120\mu s$ for all the electrical field establishments in the device. The related measurement scheme paves the way for futuristic ramp-driven InGaAs/InP APDs for detecting SWIR wavelengths under required low power consumption environments.

INDEX TERMS Adaptive optics, avalanche photodiode, LiDAR, linear mode, negative differential resistance, quenching.

I. INTRODUCTION

The avalanche photodiode (APD) exploits the carrier multiplication phenomenon to induce input signal gain resulting in high quantum efficiency, large internal gain, large dynamic range, fast response etc, finding plausibility for optical communications, lasers, single-photon detection and related fields [1], [2], [3], [4], [5], [6], [7]. The group III–V heterostructure devices e.g., InGaAs/InP having separate absorption, grading, charge, and multiplication(SAGCM) layers are the ideal candidates for the linear, and Geiger-mode applications in the short wave infrared(SWIR) wavelength range, and that even at room temperature [8], [9], [10], [11].

The associate editor coordinating the review of this manuscript and approving it for publication was Stanley Cheung.

A lot of research throughput is available offering various performance parameter enhancements e.g., reducing dark current, manipulating punch-through, and avalanche threshold voltages, enhancing multiplication factor, optimization of multiplication capability via controlling thickness, and incorporating heterojunctions/heteromaterials for tailoring electric field, reducing temporal noise, reducing afterpulsing, and avoiding accumulation, and carrier recombination at the various junctions during charge transport [12], [13], [14], [15], [16], [17], [18], [19].

Although, the InGaAs APDs dedicatedly prepared for the linear, and Geiger mode operations are structurally similar, even prepared via the same technologies or processes, but happen to be different from each other. The optimization of distinct performance attributes require different layer thicknesses, doping types or concentrations making them suitable for certain application by compromising over other features.

For illustration, linear-mode operation benefits from a high gain-bandwidth product, and as the gain-bandwidth product is inversely proportional to the width of the multiplication region (W_m), linear-mode APD design tends to emphasize thinner W_m which is way smaller than $1\mu m$. On the contrary, gain-bandwidth product has no direct impact on Geiger-mode operation. As an alternative, thicker W_m will offer lower breakdown fields resulting in negligible tunneling contributions to the dark counts, and so single photon avalanche detection(SPAD) design tends to emphasize wider W_m usually larger than $1\mu m$ [20], [21].

In this work, $1\mu m$ thick W_m being the threshold thickness, distinguishing specifically designed linear or Geiger mode APDs is intentionally incorporated, and investigated in our planar SAGCM structure InGaAs APD. It is structured in a three sub-layered InP heterojunction to explore the simultaneous plausibility of linear and Geiger modes under low-frequency ramp gating scheme. The choice of low-frequency ramp gating helps diminish afterpulsing plausibility.

We study the effect of 1310 nm photo excitation in the pre-avalanche condition of the InGaAs APD. The capability of the out-of-plane impact ionization in the specifically modified three layered heterostructure InP multiplication layer is confirmed. The InGaAs APD is set into the dynamic pre-avalanche state by applying reverse ramp gating between anode and cathode of the said planar device [22], [23], [24]. When the device is exposed to a pulsed illumination, the initial photo generated carriers experience the strong electric field, and depict the resultant photocurrent via a sharp transient decrease.

The initial charge packet resulting from the detection of weak photon burst, experience carrier multiplication enhanced signal-to-noise ratio. These carriers while passing through the readout resistor initiate an inverse quenching process which causes a decrease in the relative change in the photocurrent, and an increase in the voltage across the APD is observed.

Light detection and ranging (LiDAR) finds important applications in navigation for autonomous vehicles and spacecraft/drones, safe landing, terrain mapping, target recognition and identification, atmospheric remote sensing, and deep space exploration, thus thrusting its continuously ongoing development towards high resolution, high speed, and long range [25], [26], [27], [28], [29]. Similarly, adaptive optics systems for ground based astronomy, and space surveillance require sensors to measure the distortion of a wavefront due to atmospheric turbulence. In such systems, polarization detection with the adaptive adjustment of aperture diameter can help to improve triggering probability, and detection performance [30], [31], [32], [33]. Under surveillance applications, wavefront sensors require signal amplification to improve the signal-to-noise ratio of the embedded CCD or CMOS pixel arrays. Avalanche photodetectors operated in linear and Geiger Modes have been introduced into LiDAR, and adaptive optics systems for their capability of detecting the weakest light signal increasing measuring range, and wavefront correction capability [34], [35], [36]. Our device also has the potential of being implemented as InGaAs APD array via CMOS technology, ensuring safe-eye zone (1310 nm), reduced atmospheric attenuation, slight disturbance from Rayleigh scattering, and weak sky radiance.

The rest of this paper is organized as follows. Section II provides details of InGaAs APD fabrication processes. Section III-A comprises of the measurement scheme, and a thoughtful discussion of the possible operational physical mechanisms resulting in such counter-intuitive results extracted from our InGaAs APD, followed by (B) current-time (*I-Time*), and (C) current-voltage (*I-V*) characteristics for ramp–driven InGaAs APD under pulsed illuminations at various electric field strengths. Then, in sub-section (D) power spectral densities evaluated from (*I-Time*) curves are shown for assessing the temporal noise sources. In (E), a comprehensive discussion on overall reduced power consumption under such biasing is presented along with (F) calculations of performance parameters. In Section IV, we conclude our work.

II. DEVICE FABRICATION

With consideration for the design goals, and concepts outlined earlier, we have developed an InGaAs/InP APD illustrated in Fig. 1(a). The device design employs a SAGCM heterostructure [37]. A $1\mu m$ thick N^+ InP buffer layer ($1.0 \times 10^{17} cm^{-3}$) is grown on a $100\mu m$ thick N^+ InP substrate ($1.0 \times 10^{18} cm^{-3}$), followed by a $3\mu m$ thick undoped InGaAs($In_{0.53}Ga_{0.47}As$) absorption layer for absorbing SWIR wavelengths having a characteristic cutoff wavelength of $\sim 1.67\mu m$.

The valence band offset at an abrupt InGaAs/InP heterojunction usually results in hole trappings [38]. So, a $0.1\mu m$ thick InGaAsP grading layer ($1.0 \times 10^{16} cm^{-3}$) is inserted between the InGaAs absorber, and InP charge layers of the heterostructure to diminish the effective trap depth for

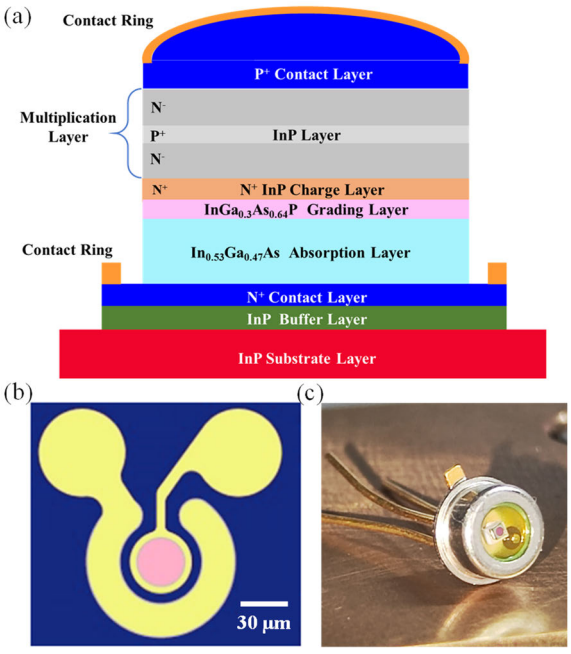

FIGURE 1. (a) An illustration showing various employed sequentially, and epitaxial grown layers having certain roles in the performance of the InGaAs APD. The metallic contact rings are also sown. (b) A high resolution micrograph of the employed InGaAs APD is incorporated while the related scale bar is 30 μm. (c) The actual InGaAs APD in the ready to test packaged form.

holes. Then, a $0.2\mu m$ thick N^+ InP epitaxial grown charge layer ($1.0 \times 10^{17} cm^{-3}$) is laid next to the grading layer to tailor the internal electric field profile in the heterostructure. The charge layer is designed to provide high electric field in the multiplication layer, and low electric field in the absorption layer, while the grading layer avoids carrier accumulation/trapping/recombination at the heterojunction interface [38].

It is followed by a three sub-layers heterostructure, collectively functioning as a $1\mu m$ thick multiplication layer, such that a $0.1\mu m$ thick P^+ InP sub-layer ($1.0 \times 10^{17} cm^{-3}$) is sandwiched between two very lightly doped or intrinsic InP sub-layers with successive thicknesses of $0.5\mu m$, and $0.4\mu m$. A double diffusion process [39] is implemented to tailor the junction profile, and create a deeper junction in the central part of the active region.

The resulting gain profile across the centeral part of the active region will be uniform while reduced in the peripheral region of the device. The final epitaxial layer is a $2\mu m$ thick undoped InP cap layer. During device fabrication, the active region is determined by the patterning of a SiN dielectric passivation layer to create a diffusion mask, and a subsequent diffusion of Zinc dopant atoms created a P^+ InP region within the undoped InP cap layer. This planar buried-junction design exploiting the high-quality SiN passivation can ensure stable, and long-life performance.

The high resolution micrograph of the employed InGaAs APD is incorporated in Fig. 1(b), where the related scale bar of 30 μm is also shown. Then, Fig.1(c) corresponds to the actual InGaAs APD in the ready to test packaged form.

III. RESULTS AND DISCUSSIONS

A. EXPERIMENTAL SETUP AND WORKING MECHANISM

Conventionally, when reverse biasing of an APD is increased, the dark current of the order of $10-100nA$ suddenly increases as punch-through voltage is reached(beyond this voltage APD operates in the linear multiplication mode, *i.e.*, impact ionization is linearly related to the input power density). The further increase of the reverse biasing beyond the avalanche threshold voltage, puts the device into Geiger mode operation where single carrier results in a significant measureable, and sustainable current level. Usually, in the Geiger mode, the APDs are operated at 5% excess voltage with reference to the threshold bias level.

The overall performance of the APD is not only decided by the design consideration but it also critically depends upon the detection circuitry that follows the APD. Quenching circuitry is necessary to quickly suppress the avalanche current by lowering the reverse bias across the APD [40].

During the onset of an avalanche process, the photo voltage across the readout resistor tends to increase, weakening the electric field present in almost all of the constituent APD layers, and particularly in the multiplication region. Then, photo voltage across the readout element that has transiently and quickly increased right after the initiation of the avalanche in the multiplication region starts deceasing through quenching phenomenon. The electric field in the multiplication region surpasses the carrier multiplication threshold again, and enables the APD for further detection of low-photon photo ionization events.

The related electrical circuitry for measuring I through the device is represented in Fig. 2(a). We have employed a rather slow passive quenching circuitry by implementing 100 kΩ resistor in series with the reverse biased InGaAs APD [41]. The series resistor functions both as quenching and readout elements by acquiring the dark/photo voltage across it. The InGaAs APD is working in the gated mode with low repetition frequency (f), *e.g.*, $1kHz$. A signal generator is implemented for gating signal V, and a synchronized pulsed signal of $10ns$ ON duration bearing $1kHz$ frequency to drive a $1310nm$ pulsed laser.

For any standard APD, various electric fields present in SAGCM layers are shown schematically in Fig.2 (b). Once, under pulsed illumination, photo ionization happens (either in linear or Geiger modes), carriers drift under various electric field strengths, and a hole initiated (blue arrow in the multiplication region) impact ionization boosts the overall photo response of the device. The red and blue dotted arrows show direction of the movement of the two carriers in the reverse bias. The holes drift toward a negatively biased anode, and electrons towards the positively biased cathode.

For our case, as shown in the left schematic of Fig.2(c), the thermally generated carriers undergo impact ionization in

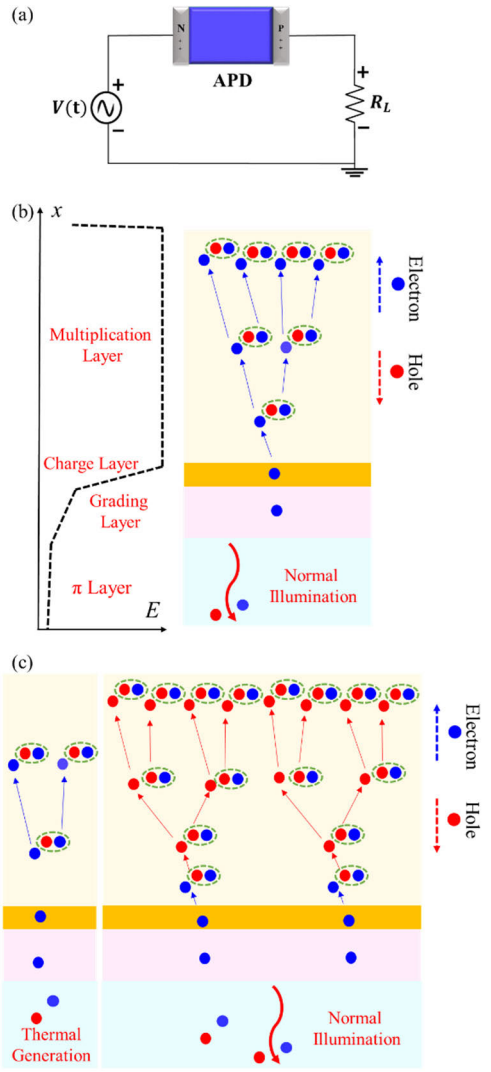

FIGURE 2. (a) A pictorial schematic of the electrical biasing scheme for the InGaAs APD is shown. A trans-impedance amplifier mimicking a $100k\Omega$ resistor R_L is connected in series with the AC input signal source V. An offset of $-35V$ is implemented for a ramp input gating signal varying between 0 *to* $-70V$ in $1ms$ time duration. (b) For any standard APD, various electric fields present in SAGCM layers are shown schematically. Once photo ionization happens under pulsed illumination, and carriers drift under various electric field strengths, hole initiated (blue arrow in the multiplication region) impact ionization will boost the overall photoresponse of the device. (c) The left side schematic emphasizes that for our InGaAs APD, thermally generated carriers will experience excessive electric field inside the multiplication region and a hole initiated linear dark avalanche will result in a steady state large background dark current. Whereas, the right side schematic demonstrates that for our InGaAs APD, photo generated carriers will experience excessive electric field inside the multiplication region, and an electron initiated linear avalanche will result in a quick reduction in the current.

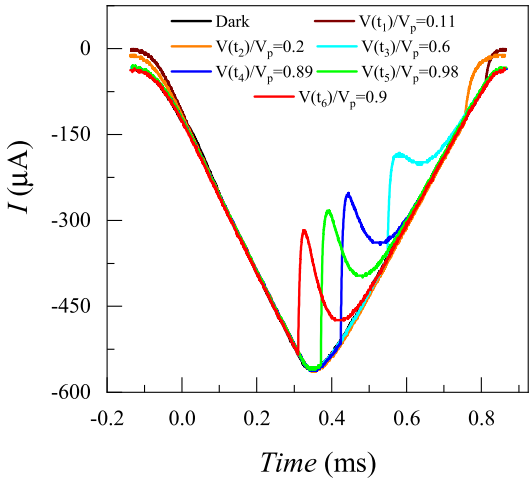

FIGURE 3. Dark and photo current curves under normal incidence of pulsed illumination are plotted over single cycle of input ramp gating V. The input ramp gating signal V varies from 0 *to* $-70V$ while frequency f for both the pulsed $1310nm$ laser, and input gating signal V is $1kHz$. The pulsed laser turns-on when ramp $V(t) = (-7.75, -14, -42, -62, -69, -62.8)V$ corresponding to $V(t_i)/V_p = (0.11, 0.2, 0.6, 0.89, 0.98, 0.9)$, while $i = 1, \ldots, 6$ and peak value of reverse bias $V_p = -70V$. Pulsed laser ON time is fixed at 10 ns for all six values of $V(t_i)/V_p$. All of the six photo-ignited impact ionization events are plotted simultaneously to understand the transient photoresponse of the InGaAs APD for pulsed illumination of $P_t = 16\mu W$.

the multiplication region, and a hole initiated dark avalanche will result in a steady state large background dark current. The huge sustainable dark current exhibits an approximately linear relationship with the gate voltage variation. After the onset of pulsed illumination onto the InGaAs APD, the multiplication region exhibits an electron dominated carrier multiplication, as shown in right schematic of Fig.2(c). This results into an overall current reduction.

This rate of reduction demonstrates a direct proportionality with the input light intensity. This sudden decrease in the initial hole dominated dark current in the electric loop corresponds to a sort of negative differential resistance incorporated in the device (this kind of current decrease is also a trademark of conventional tunnel diodes).

This sharply decreased photo voltage across the output resistor appears across InGaAs, which slowly (as passive quenching circuitry is implemented) enables the previous hole initiated dark avalanche resulting in a steady state large background dark current. This is obvious as in Fig.3, and Fig.6, large dark current signatures appear again, once passive quenching circuitry re-instates the large thermal amplified dark current following the ramp bias gating.

Our dynamic $I - t$ and $I - V$ measurements as shown in upcoming sections demonstrate a thought-provoking counter intuitive behavior compared to the conventional linear or Geiger mode operations of standard InGaAs APDs. We have discussed all of the possible foundations and physical mechanisms resulting in such behavior.

B. CURRENT VS. TIME CHARACTERISTICS

In Fig.3, current vs. time (*I-Time*), dark, and photo current curves under normal incidence 1310 nm wavelength pulsed illumination are plotted over single cycle of input ramp gating V. The ramp gating signal V varies between 0 to -70V while repetitive frequency f for both the pulsed laser and input signal V is fixed at $1kHz$. The pulsed

laser turns-on at moments in time when ramp $V(t) = (-7.75, -14, -42, -62, -69, -62.8)$V. Then, $V(t_i)/V_p$ is defined as the ratio of instant ramp gating voltage $V(t_i)$ to the peak ramp gating value $(V_p = -70\text{V})$. The plotted data belongs to $V(t_i)/V_p = (0.11, 0.2, 0.6, 0.89, 0.98, 0.9)$ where, $i = 1, \ldots, 6$. Pulsed laser ON time is set at 10 ns for all six parametric values of $V(t_i)/V_p$. This is to uniformly exploit the various electric field strengths inside the multiplication region to deduce the avalanche triggering quality of the InGaAs APD. Then, all of the photo-ignited impact ionization events are plotted simultaneously to understand the transient photoresponse of the InGaAs APD for pulsed illumination (P_t) of $16\mu W$.

The dark current level over all of the ramping cycle is very large exhibiting an approximately linear relationship with the electrical input. The possible sources of such large dark current are leakage requiring fabrication optimization, field enhanced tunneling, excessive thermal generation as device is being tested at room temperature instead of the cryogenic conditions, and high-field initiated large thermal generation rate. Moreover, the dark current due to thermally generated carriers in the regions of the device not holding sufficiently large electric field is also an important contributor. Additionally, continuously, and uniformly generated thermal carriers in the InGaAs layer successively experience generation rate dependent large linear mode avalanche in the multiplication region as the punch-through voltage of the device is only $7V$.

Once the laser is switched ON, a sudden impact-ionization initiated fast transient decrease in the absolute current value is observed. One interesting deduction from the transient photo response is the slow quenching phenomenon lasting $\sim 120\mu s$ for almost all of the photo curves belonging to all six values of $(t_i)/V_p$. This originates from the slow passive quenching circuitry ($100k\Omega$ resistor in series with the reverse biased APD) [41]. Once, photo excitation initiated photo response is quenched slowly, the same large dark condition I signature is re-established in the APD.

C. CURRENT VS. VOLTAGE CHARACTERISTICS

The transient photoresponse of the InGaAs APD which is readily set into linear mode dark avalanche via ramp gating $\boldsymbol{V}$ is discussed in terms of I vs. V characteristics as shown in Fig.4. For that, the dynamic dark, and photocurrent curves (I) under normal incidence of pulsed illumination are plotted over single sweep cycle of input voltage $\boldsymbol{V}$. Five out of the six, photo-ignited impact ionization events occur during reverse sweep $(-70\ to\ 0\ V)$ when ramp $V(t) = (-7.75, -14, -42, -62, -69,)V$ corresponding to $V(t_i)/V_p = (0.11, 0.2, 0.6, 0.89, 0.98)$ while one belonging to $V(t_6)/V_p = 0.9$ occurs in the forward sweep$(0\ to\ -70V)$.

These I vs. V characteristics are not only helpful in understanding the negative differential resistance exhibited through the quick current decrease when laser is switched-on for all six $V(t_i)/V_p$, while also depict the severe device hysterises as I curves don't overlap in the forward and reverse sweep.

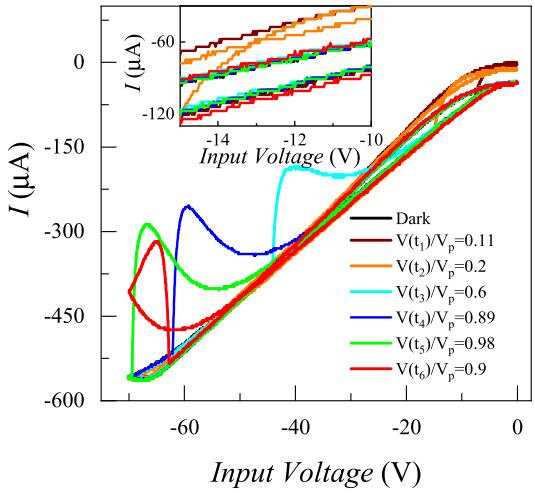

FIGURE 4. The dynamic dark, and photocurrent curves under normal incidence of pulsed illumination are plotted over single sweep cycle of input voltage V. The input ramp gating signal V varies from 0 *to* $-70V$ while repetitive frequency f for both the pulsed 1310*nm* wavelength laser, and input ramp gating signal V is 1*kHz*. The pulsed laser turns-on when ramp $V(t) = (-7.75, -14, -42, -62, -69, -62.8)$V corresponding to $V(t_i)/V_p = (0.11, 0.2, 0.6, 0.89, 0.98, 0.9)$ while $i = 1, \ldots, 6$, and peak value of reverse biasing $V_p = -70$V. Pulsed laser ON time is fixed at 10 ns for all six values of $V(t_i)/V_p$. Five out of the six photo-ignited impact ionization events occur during reverse sweep, i.e., -70 *to* 0*V*, and one corresponding to $V(t_6)/V_p = 0.9$ occurs in the forward sweep(0 *to* $-70V$).

These hysterisis are innately related to deep traps and to not very sharp junctions, as during fabrication junctions tend to diffuse, and merge due to dopants uncontrolled diffusion behaviour, and various other factors. These hysterises are more obvious at relatively low reverse biasing values as shown in the inset. For larger $V(t_i)/V_p$ values correponding to red, green, blue, and cyan colored I curves, the difference between the forward, and reverse curves reach as large as $30\mu A$. These bulit-in sources of hystersises might be the possible sources effecting the electron to hole avalanche coefficents ratio.

D. NOISE ANALYSIS

The temporal noise for the InGaAs APD being operated in low-frequency ramp gated mode can be characterized into three main parts [42]: photon shot noise, dark shot noise, and readout noise. Photon and dark shot noise originate from the intrinsic statistical nature of the generation processes in absorber layer. In contrast, the readout noise arises from charge-to-voltage conversion, and successive processing.

Fig.5 shows the respective power spectral densities (*PSD*) calculated by applying the Fast Fourier Transform (FFT) to $I - t$ signatures recorded over a complete ramp gating cycle under dark, and pulsed illuminations against $16\mu W$ corresponding to $V(t_i)/V_p = (0.11, 0.2, 0.6, 0.89, 0.98, 0.9)$. The *PSD*'s at low frequencies are prominently different owing to thermal variations, and resistive changes in the device. The *PSD*s also display white noise characteristics, demonstrating that the dominant noise sources are the readout components,

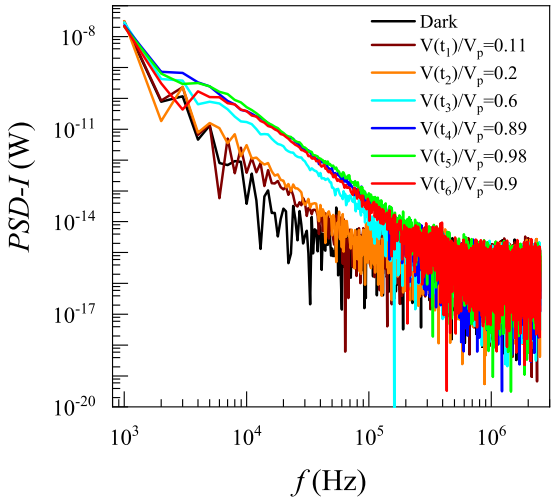

FIGURE 5. Power spectral densities (*PSD*'*s*) calculated over one complete ramp gating cycle under dark, and various pulsed illuminations of 1310 nm wavelength laser corresponding to $V(t_i)/V_p$= (0.11, 0.2, 0.6, 0.89, 0.98, 0.9) are plotted.

i.e., charge-to-current conversion by trans-impedance amplifier and oscilloscope.

At larger values of $V(t_i)/V_p$, the overall electric field inside customized $1\mu m$ thick multiplication layer in the InGaAs APD is th largest. The increase of *PSD*'s over the frequency range of 2kHz − 200kHz, corresponding to large values $V(t_i)/V_p$= (0.6, 0.89, 0.98, 0.9) is another proof that the overall system becomes more and more noisy after the onset of inherently random and schochastic avalanche phenomenon. This results from the overall noise figure increment caused by the electron-initiated avalanche process in the multiplication layer, and pulsed laser shot noise.

The large values of *PSDs* are inherently related to deep traps, merged and diffused device junctions, and a large background linear-mode thermal hole initiated dark avalanche current. But, the overall reduction of the absolute value of I following the photo-ignited avalanche process, endorses the changes in the ratio of electron to hole avalanche coefficients. The avalanche triggering capability of the APD and the quantification of avalanche multiplication are correlated by the self-quenching, and quenching mechanisms. Further investigation is needed to understand to what extent these self-quenching, and quenching mechanisms can be used to reduce the stochastic attribute of impact ionization.

E. POWER CONSUMPTION IN RAMP-DRIVEN VS. SINUSOIDAL-DRIVEN INGAAS APDS

The power consumption in the InGaAs APD comprises of photo-sensing (photo generation in the InGaAs absorber layer), high electric field requirements in InP multiplication layer for initiating avalanche, and to drive the successive readout circuitry. As obvious, the energy dissipation in the loop is directly related input voltage V.

To reduce P_{APD} which is the power consumed during APD operation, gating signal type, and its peak values are the factors to be considered. From our estimates, the involved processes under ramp biasing, dissipate smaller power when compared with the sinusoidally-driven InGaAs APD [43], [44].

For a simple series RC circuit biased with zero offset sinusoidal, and ramp input V signals, the root-mean-square values of an alternating current, which are its relevant DC equivalents, are $\frac{I_p}{2}$ and $\frac{I_p}{\sqrt{3}}$, respectively, where I_p is the peak value of the current. Then, the effective power dissipated in the loop for zero offset sinusoidal, and ramp input V signals will be $I_p^2R/2$, and $I_p^2R/3$(two third of the sinusoidal bias counterpart), respectively.

We did not bias the InGaAs APD via a zero-offset ramp V_g. Instead: a dc offset of $V_{DC} = -35$V is implemented, as the electrical ramp gating signal varies between 0V, and −70V. Thus, the effective P_{APD} in the photo-sensing mode for the ramp signal V will be $\left(I_{DC}^2 + \frac{I_p^2}{3}\right)R$, which is smaller than $\left(I_{DC}^2 + \frac{I_p^2}{2}\right)R$ for the sinusoidal signal having the same peak-to-peak voltage. Here, I_{DC} is the constant reverse-biased dark current flowing in the device due to V_{DC}, and I_p corresponds to $V_p = -70$V.

F. PARAMETER CALCULATIONS

For InGaAs absorbing material, the absorption coefficient at 1310 nm wavelength happens to be $11500cm^{-1}$. The photo generation in the normal incidence direction exhibits a decaying exponential signature with the maximum at the InGaAsP grading, and InGaAs absorber layers interface. The $1/e$ of the maximum generation lies at $\sim 1.23\mu m$ away from the interface into the absorber layer. Hence, for our absorption layer of $3\mu m$ thickness, 82.5% of incident P_t is absorbed as effective $e-h$ pair generation, and about 17.5% of transmits through the absorber layer.

An approximately linear external quantum efficiency (EQE) while InGaAs APD is electrically biased with ramp gating corresponding to $V(t_i)/V_p$ = (0.11, 0.2, 0.6, 0.89, 0.9, 0.98) values under $16\mu W$ pulsed illumination originates from the inherently persistent linear avalanche mode characterized for the APD. Although, the background thermally generated charge is being continuously, steadily, and linearly multiplied. But, still the photo responses under pulsed illuminations are distinguishable from the dark current depicting the capability of the device to multiply even in this compromised linear multiplication mode.

The punch-through voltage of the APD being only 7V, and then a persistent linear multiplication trend following linear relationship with the increasing ramp gating is primarily different from usual APDs. Herein, avalanche threshold voltage after which the device sets itself in the Geiger mode operation is very large. This is quite understandable as the multiplication layer width is $1\mu m$, which is neither a standard width for linear or Geiger mode. The inset of Fig.6 shows the

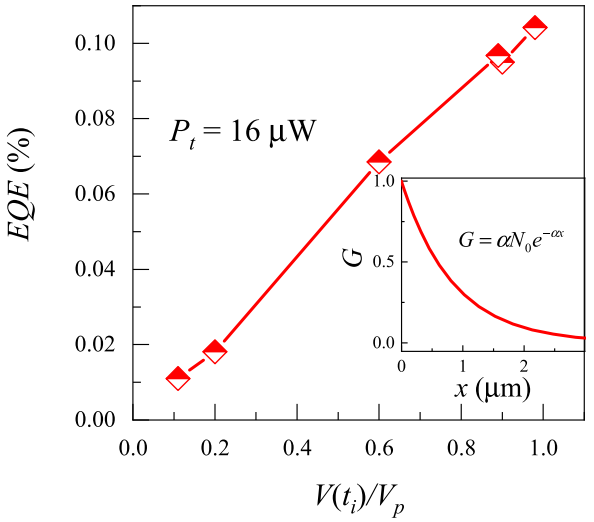

FIGURE 6. External Quantum Efficiency (*EQE*) calculated from transient photo response measurements of *I* while InGaAs APD is set into dark linear avalanche condition by low frequency ramp gating signal, and exposed to 16μW illumination at $V(t_i)/V_p$ = (0.11, 0.2, 0.6, 0.89, 0.9, 0.98). The inset plots the normalized generation rate (*G*) in the InGaAs absorber layer. Approximately 17.5 % of the pulse illumination transmits while other is absorbed, and takes part in the electron-initiated carrier multiplication in the InP multiplication layer

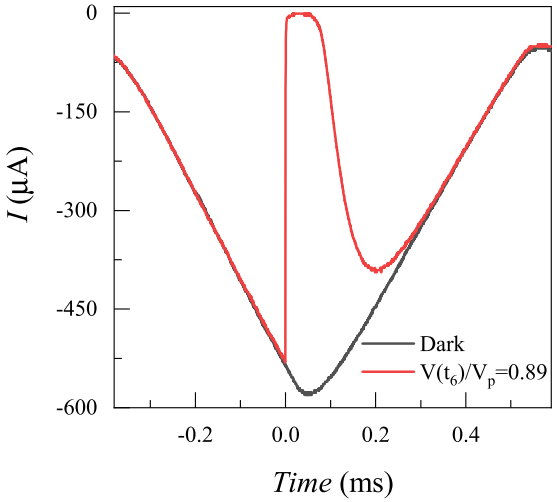

FIGURE 7. The dark, and a photo current curves under a pulsed illumination of $P_t = 28\mu W$ are plotted over single cycle of input ramp gating *V*. The pulsed laser turns-on at moment in time when ramp $V(t) = -62.8$V corresponding to $V(t_6)/V_p = 0.89$.

relevant normalized generation rate (G). The related formulas are also mentioned, where α is the generation rate, and x is the distance relevant to the interface of absorber layer.

In Fig.7, *I-Time* data for the dark, and a photo current curve for 28μW pulsed normal incidence illumination is plotted over one cycle of input ramp gating V. The pulsed laser turns-on at a moment in time when ramp $V(t) = -62.8$ V corresponding to $V(t)/V_p = 0.89$. This is the most interesting scenario in which the onset of electron initiated carrier multiplication results in internal electric field tailoring such that photo voltage across the resistor becomes almost negligible. The overall applied voltage appears across the InGaAs APD, and device reinstates the previous thermal hole initiated dark avalanche in $\sim 200\mu s$, once the rather slow photo response has been quenched.

The observed quenching in our InGaAs APD is a sort of inverse quenching when compared with the conventional InGaAs APDs. As discussed earlier, I signatures at zero biasing exhibit a non-zero current level. But if the impinged illumination is increased, and a huge bulk of electrons is sunk in the opposite direction with reference to holes, a complete compensation of all of the built-in sources of hysteresis can be established.

The low frequency ramp drive implemented in our testing scheme is more suitable for applications like surveillance, adaptive optics, and LiDAR, where control of power dissipation is more critical than linearity of operation [45], [46], [47], [48].

IV. CONCLUSION

A 1μm thick InP multiplication layer, specifically designed in the form of three sub-layers heterostructure in a SAGCM configuration InGaAs APD is probed for 1310 nm pulsed light. The linear and Geiger mode applications of the APDs require much thinner, and thicker multiplication regions with 1μm being the reference thickness, separating the two modes in context of structural optimization. An interesting phenomenon of light-induced changes in the intrinsic values of avalanche coefficients for electrons, and holes is observed resulting in negative differential resistance incorporation. This resultantly establishes an inverse quenching behavior of the passive readout circuitry by offering a positive feedback when compared with usual APDs operation. The reverse biased APD is exploited for synchronous photo-generation events under various electric field strengths established by the low frequency ramp gating signal. Linear mode operation is extended while linear multiplication capability is much enhanced, suggesting an interesting blend of linear and Geiger modes. The proposed device and measurement scheme is more suitable for applications like surveillance, adaptive optics, and LiDAR where control of power dissipation is more critical than linearity of operation.

ACKNOWLEDGMENT

(Afshan Khaliq, Xinyi Zhou, and Hongyu Chai contributed equally to this work.)

REFERENCES

[1] S. Assefa, F. Xia, and Y. A. Vlasov, "Reinventing germanium avalanche photodetector for nanophotonic on-chip optical interconnects," *Nature*, vol. 464, no. 7285, pp. 80–84, Mar. 2010, doi: 10.1038/nature08813.

[2] J. Michel, J. Liu, and L. C. Kimerling, "High-performance Ge-on-Si photodetectors," *Nature Photon.*, vol. 4, no. 8, pp. 527–534, Aug. 2010, doi: 10.1038/nphoton.2010.157.

[3] Y. Li, X. Liu, X. Li, L. Zhang, B. Chen, Z. Zhi, X. Li, G. Zhang, P. Ye, G. Huang, D. He, W. Chen, F. Gao, P. Guo, X. Luo, G. Lo, and J. Song, "Germanium-on-silicon avalanche photodiode for 1550 nm weak light signal detection at room temperature," *Chin. Opt. Lett.*, vol. 20, no. 6, 2022, Art. no. 062501, doi: 10.3788/col202220.062501.

[4] H. Han, Y. Zhu, Z. Guo, Z. Li, H. Qu, W. Gao, D. Wang, and W. Wang, "High performance InGaAs/InP avalanche photodiode integrated with metal-insulator-metal microcavity," *Opt. Quantum Electron.*, vol. 53, no. 6, pp. 1–9, Jun. 2021, doi: 10.1007/s11082-021-02915-x.

[5] J. C. Campbell, A. G. Dentai, W. S. Holden, and B. L. Kasper, "High-speed InP/InGaAsP/InGaAs avalanche photodiodes," in *IEDM Tech. Dig.*, Dec. 1983, pp. 464–467, doi: 10.1109/iedm.1983.190543.

[6] P. Martyniuk, P. Wang, A. Rogalski, Y. Gu, R. Jiang, F. Wang, and W. Hu, "Infrared avalanche photodiodes from bulk to 2D materials," *Light, Sci. Appl.*, vol. 12, no. 1, p. 212, Aug. 2023, doi: 10.1038/s41377-023-01259-3.

[7] X. Jiang, M. A. Itzler, R. Ben-Michael, and K. Slomkowski, "InGaAsP-InP avalanche photodiodes for single photon detection," *IEEE J. Sel. Topics Quantum Electron.*, vol. 13, no. 4, pp. 895–905, 2007, doi: 10.1109/JSTQE.2007.903001.

[8] J. C. Campbell, "Recent advances in avalanche photodiodes," *J. Lightw. Technol.*, vol. 34, no. 2, pp. 278–285, Jan. 15, 2016, doi: 10.1109/JLT.2015.2453092.

[9] J. C. Campbell, "Recent advances in telecommunications avalanche photodiodes," *J. Lightw. Technol.*, vol. 25, no. 1, pp. 109–121, Jan. 2007, doi: 10.1109/JLT.2006.888481.

[10] A. Lacaita, P. A. Francese, F. Zappa, and S. Cova, "Performance of commercially available germanium photodiodes," *Appl. Opt.*, vol. 33, no. 30, p. 6902, 1994.

[11] P. A. Hiskett, G. S. Buller, A. Y. Loudon, J. M. Smith, I. Gontijo, A. C. Walker, P. D. Townsend, and M. J. Robertson, "Performance and design of InGaAs/InP photodiodes for single-photon counting at 1.55 μm," *Appl. Opt.*, vol. 39, no. 36, p. 6818, 2000, doi: 10.1364/ao.39.006818.

[12] Y. Zhao and J. Chen, "InGaAs/InP SAGCM avalanche photodiode with a heterojunction multiplication layer," *Phys. B, Condens. Matter*, vol. 629, Mar. 2022, Art. no. 413637, doi: 10.1016/j.physb.2021.413637.

[13] Y. Jiang and J. Chen, "Optimization of the linearity of InGaAs/InAlAs SAGCM APDs," *J. Lightw. Technol.*, vol. 37, no. 14, pp. 3459–3464, Jul. 15, 2019, doi: 10.1109/JLT.2019.2917262.

[14] D. Haško, J. Kováč, F. Uherek, J. Škriniarová, J. Jakabovič, and L. Peternai, "Avalanche photodiode with sectional InGaAsP/InP charge layer," *Microelectron. J.*, vol. 37, no. 6, pp. 483–486, Jun. 2006, doi: 10.1016/j.mejo.2005.09.008.

[15] S. MohammadNejad and F. Aghaei, "Noise characteristics improvement of submicron InP/InGaAs avalanche photodiode for laser detection system," *Opt. Commun.*, vol. 455, Jan. 2020, Art. no. 124561, doi: 10.1016/j.optcom.2019.124561.

[16] M. A. Khamis, W. E. Rashid, P. J. Ker, and K. Y. Lau, "Effect of multiplication and absorption layers width on avalanche multiplication gain in InGaAs/InP avalanche photodiode," *Int. J. Eng. Technol.*, vol. 7, no. 4.35, p. 559, Nov. 2018, doi: 10.14419/ijet.v7i4.35.22909.

[17] M. Ren, Y. Liang, X. Gu, W. Kong, E. Wu, G. Wu, and H. Zeng, "A 1550-nm time-of-flight laser ranging system based on 1-GHz sine-wave gated InGaAs/InP APD," in *Proc. Conf. Lasers Electro-Opt.*, 2012, pp. 16–17.

[18] N. Calandri, M. Sanzaro, A. Tosi, and F. Zappa, "Charge persistence in InGaAs/InP single-photon avalanche diodes," *IEEE J. Quantum Electron.*, vol. 52, no. 3, pp. 1–7, Mar. 2016, doi: 10.1109/JQE.2016.2526608.

[19] D. Hasko, F. Uherek, J. Kovac, J. Jakabovic, J. Skriniarova, and L. Peternai, "Utilization of InGaAsP charge layer in InGaAs/InP SACM APD," in *Proc. 5th Int. Conf. Adv. Semiconductor Devices Microsystems*, Oct. 2004, pp. 13–16, doi: 10.1109/ASDAM.2004.1441146.

[20] D. A. Ramirez, M. M. Hayat, G. Karve, J. C. Campbell, S. N. Torres, B. E. A. Saleh, and M. C. Teich, "Detection efficiencies and generalized breakdown probabilities for nanosecond-gated near infrared single-photon avalanche photodiodes," *IEEE J. Quantum Electron.*, vol. 42, no. 2, pp. 137–145, Feb. 2006, doi: 10.1109/JQE.2005.861627.

[21] J. P. Donnelly, E. K. Duerr, K. A. Mcintosh, E. A. Dauler, D. C. Oakley, S. H. Groves, C. J. Vineis, L. J. Mahoney, K. M. Molvar, P. I. Hopman, K. E. Jensen, G. M. Smith, S. Verghese, and D. C. Shaver, "Design considerations for 1.06-μm InGaAsP-InP Geiger-mode avalanche photodiodes," *IEEE J. Quantum Electron.*, vol. 42, no. 8, pp. 797–809, Aug. 2006, doi: 10.1109/JQE.2006.877300.

[22] L. F. Lou and G. L. Tettemer, "Characterization of metal-oxide-semiconductor capacitors with a fast-ramp technique," *J. Appl. Phys.*, vol. 63, no. 11, pp. 5398–5405, Jun. 1988, doi: 10.1063/1.340358.

[23] L. F. Lou and G. L. Tettemer, "An experimental study of a metal-oxide-semiconductor photomultiplier," *J. Appl. Phys.*, vol. 66, no. 6, pp. 2678–2688, Sep. 1989, doi: 10.1063/1.344237.

[24] A. Aal, "Fast wafer level reliability assessment of ultra thick oxides under impact ionization conditions," in *Proc. IEEE Int. Integr. Rel. Workshop Final Rep.*, Oct. 2007, pp. 117–120, doi: 10.1109/IRWS.2007.4469235.

[25] Y. Jiang, S. Karpf, and B. Jalali, "Time-stretch LiDAR as a spectrally scanned time-of-flight ranging camera," *Nature Photon.*, vol. 14, no. 1, pp. 14–18, Jan. 2020, doi: 10.1038/s41566-019-0548-6.

[26] G. G. Gimmestad and D. W. Roberts, "1.5 microns: The future of unattended aerosol LiDAR?" in *Proc. Int. Geosci. Remote Sens. Symp.*, Sep. 2004, pp. 1944–1946, doi: 10.1117/12.602582.

[27] J. Tachella, Y. Altmann, N. Mellado, A. McCarthy, R. Tobin, G. S. Buller, J.-Y. Tourneret, and S. McLaughlin, "Real-time 3D reconstruction from single-photon LiDAR data using plug-and-play point cloud denoisers," *Nature Commun.*, vol. 10, no. 1, pp. 1–6, Nov. 2019, doi: 10.1038/s41467-019-12943-7.

[28] C. Tan, W. Kong, G. Huang, J. Hou, Y. Luo, T. Chen, X. Liu, and R. Shu, "Long-range daytime 3D imaging LiDAR with short acquisition time based on 64 × 64 Gm-APD array," *IEEE Photon. J.*, vol. 14, no. 3, pp. 1–7, Jun. 2022, doi: 10.1109/JPHOT.2022.3166807.

[29] S. Wu, X. Zhai, and B. Liu, "Aircraft wake vortex and turbulence measurement under near-ground effect using coherent Doppler LiDAR," *Opt. Exp.*, vol. 27, no. 2, p. 1142, 2019, doi: 10.1364/oe.27.001142.

[30] B. Aull, "Geiger-mode avalanche photodiode arrays integrated to all-digital CMOS circuits," *Sensors*, vol. 16, no. 4, p. 495, Apr. 2016, doi: 10.3390/s16040495.

[31] F. Soldevila, E. Salvador-Balaguer, P. Clemente, E. Tajahuerce, and J. Lancis, "High-resolution adaptive imaging with a single photodiode," *Sci. Rep.*, vol. 5, no. 1, pp. 1–9, Sep. 2015, doi: 10.1038/srep14300.

[32] X. Zhou, J. Sun, Z. Fan, S. Li, and W. Lu, "Research on detection performance improvement of polarization GM-APD LiDAR with adaptive adjustment of aperture diameter and spatial correlation method," *Opt. Laser Technol.*, vol. 155, Nov. 2022, Art. no. 108400, doi: 10.1016/j.optlastec.2022.108400.

[33] B. F. Aull, D. R. Schuette, R. K. Reich, R. L. Johnsonb, and W. St, "Adaptive optics wavefront sensors based on photon-counting detector arrays," *Proc. SPIE*, vol. 7736, Jul. 2010, Art. no. 773610.

[34] T. Mizuno, H. Ikeda, K. Makino, Y. Tamura, Y. Suzuki, T. Hashi, T. Baba, S. Adachi, and R. Okumura, "InGaAs Geiger-mode three-dimensional image sensor for flash LiDAR," *J. Soc. Inf. Display*, vol. 31, no. 4, pp. 158–168, Apr. 2023, doi: 10.1002/jsid.1196.

[35] Y. Liang, B. Xu, Q. Fei, W. Wu, X. Shan, K. Huang, and H. Zeng, "Low-timing-jitter GHz-gated InGaAs/InP single-photon avalanche photodiode for LiDAR," *IEEE J. Sel. Topics Quantum Electron.*, vol. 28, no. 2, pp. 1–7, Mar. 2022, doi: 10.1109/JSTQE.2021.3109584.

[36] Z. Li, Z. Bao, Y. Shi, B. Feng, E. Wu, G. Wu, and H. Zeng, "Photon-counting chirped amplitude modulation LiDAR with 1.5-GHz gated InGaAs/InP APD," *IEEE Photon. Technol. Lett.*, vol. 27, no. 6, pp. 616–619, Mar. 15, 2015, doi: 10.1109/LPT.2014.2386354.

[37] K. Nishida, K. Taguchi, and Y. Matsumoto, "InGaAsP heterostructure avalanche photodiodes with high avalanche gain," *Appl. Phys. Lett.*, vol. 35, no. 3, pp. 251–253, Aug. 1979, doi: 10.1063/1.91089.

[38] M. A. Itzler, R. Ben-Michael, C..-F. Hsu, K. Slomkowski, A. Tosi, S. Cova, F. Zappa, and R. Ispasoiu, "Single photon avalanche diodes (SPADs) for 1.5 μm photon counting applications," *J. Mod. Opt.*, vol. 54, nos. 2–3, pp. 283–304, Jan. 2007, doi: 10.1080/09500340600792291.

[39] Y. Liu, S. R. Forrest, J. Hladky, M. J. Lange, G. H. Olsen, and D. E. Ackley, "A planar InP/InGaAs avalanche photodiode with floating guard ring and double diffused junction," *J. Lightw. Technol.*, vol. 10, no. 2, pp. 182–193, Feb. 1992, doi: 10.1109/50.120573.

[40] S. Cova, M. Ghioni, A. Lacaita, C. Samori, and F. Zappa, "Avalanche photodiodes and quenching circuits for single-photon detection," *Appl. Opt.*, vol. 35, no. 12, p. 1956, 1996, doi: 10.1364/ao.35.001956.

[41] J. G. Rarity, T. E. Wall, K. D. Ridley, P. C. M. Owens, and P. R. Tapster, "Single-photon counting for the 1300–1600-nm range by use of peltier-cooled and passively quenched InGaAs avalanche photodiodes," *Appl. Opt.*, vol. 39, no. 36, p. 6746, 2000, doi: 10.1364/ao.39.006746.

[42] K. Irie, A. E. McKinnon, K. Unsworth, and I. M. Woodhead, "A technique for evaluation of CCD video-camera noise," *IEEE Trans. Circuits Syst. Video Technol.*, vol. 18, no. 2, pp. 280–284, Feb. 2008, doi: 10.1109/TCSVT.2007.913972.

[43] M. Ren, Y. Liang, W. Sun, G. Wu, J. C. Campbell, and H. Zeng, "Timing response of sinusoidal-gated Geiger mode InGaAs/InP APD," *IEEE Photon. Technol. Lett.*, vol. 26, no. 17, pp. 1762–1765, Sep. 2014, doi: 10.1109/LPT.2014.2334057.

[44] J. Li, R. Huang, A. P. Morrison, M. Chen, C. Teng, Y. Cheng, L. Yuan, Y. Shi, and S. Deng, "Design of a room-temperature, sine-wave gated, InGaAs/InP SPAD based photon counting system with dead-time mitigation," *J. Lightw. Technol.*, vol. 42, no. 8, pp. 2887–2893, Apr. 15, 2024, doi: 10.1109/JLT.2023.3332480.

[45] M. F. Tompsett, "The quantitative effects of interface states on the performance of charge-coupled devices," *IEEE Trans. Electron Devices*, vol. ED-20, no. 1, pp. 45–55, Jan. 1973, doi: 10.1109/t-ed.1973.17607.

[46] C. Mackay, R. Rebolo-López, B. F. Castellá, J. Crass, D. L. King, L. Labadie, P. Aisher, A. P. Garrido, M. Balcells, A. Díaz-Sánchez, J. J. Fuensalida, R. L. Lopez, A. Oscoz, J. A. P. Prieto, L. F. Rodríguez-Ramos, and I. Villó, "AOLI: Adaptive optics lucky imager: Diffraction limited imaging in the visible on large ground-based telescopes," *Proc. SPIE*, vol. 8446, May 2014, Art. no. 844621, doi: 10.1117/12.925618.

[47] P. J. Pool, D. G. Morris, D. J. Burt, R. T. Bell, A. D. Holland, and D. R. Smith, "Application of electron multiplying CCD technology in space instrumentation," *Proc. SPIE*, vol. 5902, Jan. 2005, Art. no. 59020, doi: 10.1117/12.621627.

[48] U. Mallik, P. Petrone, and D. J. Benford, "Maturing electron multiplying charge coupled device photon-counting with variable multiplication gain imaging for a coronagraphic instrument," *J. Astronomical Telescopes, Instrum., Syst.*, vol. 5, no. 4, p. 1, Oct. 2019, doi: 10.1117/1.jatis.5.4.045001.

AFSHAN KHALIQ received the M.S. degree in physics from Pakistan Institute of Engineering and Applied Sciences, in 2013, and the Ph.D. degree in electronic science and technology from Zhejiang University, Hangzhou, China, in 2022. She is currently a Postdoctoral Research Fellow with the Department of Physics, Zhejiang Normal University, Jinhua, China. She is also working in collaboration with Hangzhou City University. Her research interests include designing and simulating novel nanoscale semiconductor devices, design and fabrication of III—V materials-based avalanche photodiodes, and 2D material-based heterostructure photovoltaic devices.

XINYI ZHOU received the B.S. degree in electronic information from Hangzhou City University, Hangzhou, China, in 2023. His research interest includes the testing and analysis of InGaAs-based avalanche photodiodes.

HONG-YU CHAI received the B.S. degree in electronic science and technology from Xidian University, Xi'an, China, in 2010, and the Ph.D. degree in optical engineering from Beijing University of Posts and Telecommunications, Beijing, China, in 2017. He is currently an Assistant Research Fellow with the Institute of Semiconductors, Chinese Academy of Sciences, Beijing. His research interests include optical communications, quantum dot materials, and semiconductor laser devices.

MUNIR ALI received the B.S. and M.S. degrees in electronics from Quaid-i-Azam University, Islamabad, Pakistan, in 2011, and the Ph.D. degree from the School of Micro-Nano Electronics, Zhejiang University, Hangzhou, China, in 2023. He spent six years as a Lecturer, teaching various avionics-related subjects. His research interests include carrier multiplication in III-V heterostructures, Ge-on-Si devices, and 2D/3D materials-based heterostructures, having the potential of combining the merits of CCD and CMOS imaging technologies.

HAO WU received the B.S. degree from the College of Materials and Chemistry, China Jiliang University, Hangzhou, China, in 2018, and the Ph.D. degree from the College of Optical Science and Engineering, Zhejiang University, Hangzhou, in 2023. He is currently a Postdoctoral Research Fellow with Hangzhou City University, Hangzhou. His research interests include the design and fabrication of ultraviolet optoelectronic devices based on 2D materials and low-dimensional III-V semiconductors.

OUSSAMA GASSAB (Member, IEEE) was born in Djelfa, Algeria. He received the B.Sc. degree in electrical and electronic engineering and the M.Sc. degree in telecommunications from the National Institute of Electrical and Electronic Engineering, Boumerdes, Algeria, in 2013 and 2015, respectively, and the Ph.D. degree in electrical engineering (electromagnetic compatibility—EMC) from Shanghai Jiao Tong University, Shanghai, China, in 2020. From 2021 to 2023, he was a Postdoctoral Research Fellow with the Department of Information Science and Electronic Engineering, Zhejiang University, Hangzhou, China. He is currently a Researcher with the School of Information and Electrical Engineering, Hangzhou City University, Hangzhou, and the Department of Information Science and Electronic Engineering, Zhejiang University, Hangzhou. His research interests include EMC, antenna array design, distributed parameter circuit modeling, statistical models for the characterization of interference effects, high-speed cable modeling, shielding effectiveness, power electronics, mathematics, and modern physics. He was a recipient of a Research Fund for International Young Scientists and the National Zhejiang Provincial Fund, in 2022. He is currently a Reviewer of several international journals, including IEEE Transactions and IEEE Letters. He was selected as a Distinguished Reviewer of IEEE Transactions on Electromagnetic Compatibility, in 2022.

HONG LIU received the B.E. degree from Hefei University of Technology, Hefei, China, in 2000, and the Ph.D. degree from Zhejiang University, Hangzhou, China, in 2006. He is currently an Associate Professor with Hangzhou City University, Hangzhou. His research interest includes the design methodology of electronic design automation (EDA) for chip-package-PCB systems.

DUO XIAO received the B.E. degree in radio technology from Wuhan University, Wuhan, China, in 1990, and the M.S. degree in communication and information systems from Huazhong University of Science and Technology, Wuhan, in 2001. He is currently a Professor with Hangzhou City University, Hangzhou, China. His research interest includes multiphysics modeling and simulation.

XIAO-GUANG YANG received the B.S. and M.S. degrees in physics from Northwestern Polytechnical University, in 2005 and 2008, respectively, and the Ph.D. degree in electronic engineering from the Institute of Semiconductors, Chinese Academy of Sciences (IOSCAS), in 2011. He is currently a Professor with IOSCAS and the University Chinese Academy of Sciences (UCAS) and the Deputy Director of the Key Laboratory of Semiconductor Materials Science, CAS. His research interest includes low-dimensional III-V compound materials and related devices.

SICHAO DU received the B.S. degree in materials physics from Northwestern Polytechnical University, Xi'an, China, in 2005, the M.Phil. degree in optoelectronics devices and materials from The Australian National University, Australia, in 2009, and the Ph.D. degree in optoelectronics devices and materials from The University of Sydney, Australia, in 2014. He is currently an Associate Professor with Hangzhou City University, Hangzhou, China. His research interests include the design and fabrication of ultrasensitive optoelectronic devices based on 2D materials and low-dimensional III-V semiconductors.